Electronic Supporting Information file

Click Chemistry in Carbon Nanoreactors

Graham A. Rance, William A. Solomonsz, Andrei N. Khlobystov

School of Chemistry, University of Nottingham, University Park, Nottingham, UK

S1. General experimental

All reagents, including alkynes **1c**, **1d**, **1e**, **1f**, **1g** and **1h** and azide **2b**, were purchased from Sigma-Aldrich, UK and used without further purification. Alkynes **1a**[S1] and **1b**[S2] and azide **1b**[S3] were synthesised according to literature protocols. Graphitised carbon nanofibres (Pyrograf PR-24) were purchased from Applied Science, USA. All glassware was cleaned with a mixture of hydrochloric and nitric acid (3:1 v/v, 'aqua regia') and rinsed thoroughly with deionised water, cleaned with potassium hydroxide in isopropyl alcohol and finally rinsed thoroughly with deionised water. ^{1}H and ^{13}C NMR spectra were obtained using a Bruker DPX-300 (300.13 and 75.4761 MHz respectively) spectrometer at 298K using C_6D_6, $CDCl_3$ or CD_3OD as the solvent. Attenuated total reflectance infra-red spectra were measured using a Nicolet 380 FT-IR spectrometer over the range 4000-600 cm^{-1}. UV-vis spectra were recorded in solution using 1 cm quartz cuvettes using a Perkin-Elmer Lambda 25 UV-vis spectrophotometer at a scan rate of 480 nm min^{-1} over the range 350-900 nm. Mass spectrometry was conducted on a Bruker Apex IV using ESI in positive mode. Thermogravimetric analysis was performed using a TA Instruments SDT Q600 under a flow of air at a rate of 90 mL min^{-1} at a heating rate of 10 ^{o}C min^{-1} from room temperature to 1000 ^{o}C. Transmission electron microscopy was performed using a JEOL 2100F TEM (field emission gun source, information limit < 0.19 nm) at room temperature. Nanoparticle size analysis was conducted using Gatan DigitalMicrograph software. Energy dispersive X-ray analysis was performed using an Oxford Instruments INCA 560 X-ray microanalysis system. Samples were prepared via drop-drying methanolic solutions onto a copper grid mounted "lacey" carbon films. X-ray photoelectron spectra were recorded using a Kratos AXIS ULTRA with monochromated Al Kα radiation (10 kV anode potential, 15 A emission current) in fixed analyser transmission mode (80 eV pass energy).

S2. Synthesis and characterisation of nanoparticles

Preparation of copper nanoparticles

The preparation of copper nanoparticles was conducted in a method analogous to that described by Garitaonandia *et al.*[S4] and is based on a modified Brust-Schiffrin reduction.[S5] To an aqueous solution of copper nitrate hemipentahydrate (140 mg, 0.6 mmol, 1.0 eq.) in deionised water (60 mL) was added a solution of tetraoctylammonium bromide (2.19 g, 4 mmol, 6.7 eq.) in toluene (160 mL) and the combined mixture stirred at room temperature for 10 min. To this was added a solution of dodecanethiol (216 µL, 0.9 mmol, 1.5 eq.) in toluene (2 mL) and the combined mixture stirred at room temperature for 10 min. To this was added dropwise a solution of sodium borohydride (378 mg, 10 mmol, 16.7 eq.) in deionised water (50 mL) and the combined mixture stirred at room temperature for 16 hr. The phases were separated, the organic phase washed with deionised water (3 x 100 mL), dried over anhydrous sodium sulphate and the solvent concentrated to approximately 5 mL *in vacuo*. To this was added acetone (450 mL) and the product precipitated at -30 °C over 16 hr, collected by vacuum filtration (0.45 µm, PTFE), washed with ethanol (300 mL) and acetone (300 mL) and dried under vacuum to yield a grey solid (68.9 mg).

Preparation of copper-silver alloy nanoparticles

The preparation of copper nanoparticles was conducted in a method analogous to that described by Ang *et al.*[S6] To a mixed aqueous solution of copper nitrate hemipentahydrate and silver nitrate (0.2 mmol total, 1.0 eq.) in deionised water (30 mL) was added a solution of tetraoctylammonium bromide (0.49 g, 1.5 mmol, 7.5 eq.) in toluene (80 mL) and the combined mixture stirred at room temperature for 10 min. To this was added a solution of dodecanethiol (44 µL, 0.2 mmol, 1 eq.) and the combined mixture stirred at room temperature for 10 min. To this was added dropwise a solution of sodium borohydride (84 mg, 2.2 mmol, 11.0 eq.) in deionised water (25 mL) and the combined mixture stirred at room temperature for 16 hr. The phases were separated, the organic phase washed with deionised water (3 x 50 mL), dried over anhydrous sodium sulphate and the solvent concentrated to approximately 5 mL *in vacuo*. To this was added acetone (450 mL) and the product precipitated at -30 °C over 16 hr, collected by vacuum filtration (0.45 µm, PTFE), washed with ethanol (300 mL) and acetone (300 mL) and dried under vacuum to yield a brown solid (28.0, 27.3 and 27.3 mg for 75:25, 50:50 and 25:75 ratios of Cu:Ag respectively).

Preparation of silver nanoparticles

The preparation of silver nanoparticles was conducted in a method analogous to that described by Garitaonandia *et al.*[S4] To an aqueous solution of silver nitrate (32 mg, 0.2 mmol, 1.0 eq.) in deionised water (30 mL) was added a solution of tetraoctylammonium bromide (0.49 g, 1.5 mmol, 7.5 eq.) in toluene (80 mL) and the combined mixture stirred at room temperature for 10 min. To this was added a solution of dodecanethiol (44 µL, 0.2 mmol, 1 eq.) and the combined mixture stirred at room temperature for 10 min. To this was added dropwise a solution of sodium borohydride (84 mg, 2.2 mmol, 11.0 eq.) in deionised water (25 mL) and the combined mixture stirred at room temperature for 16 hr. The phases were separated, the organic phase washed with deionised water (3 x 50 mL), dried over anhydrous sodium sulphate and the solvent concentrated to approximately 5 mL *in vacuo*. To this was added acetone (450 mL) and the product precipitated at -30 °C over 16 hr, collected by vacuum filtration (0.45 µm, PTFE), washed with ethanol (300 mL) and acetone (300 mL) and dried under vacuum to yield a brown solid (34.0 mg).

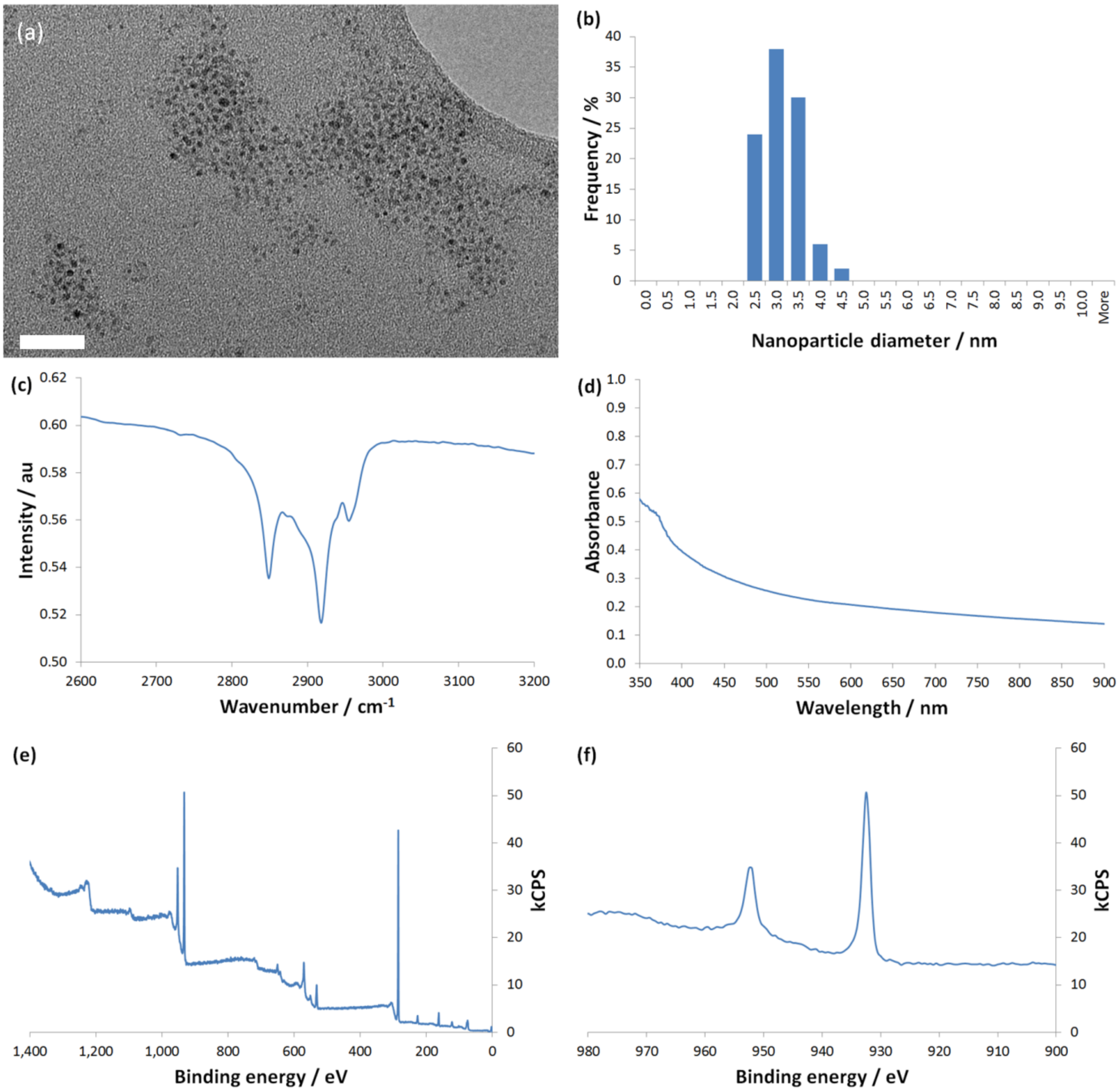

Figure S1. Characterisation of CuNP produced by the Brust-Schiffrin reduction. Transmission electron microscopy (a) and the corresponding diameter analysis histogram (b) show that the nanoparticles are small, largely spherical and have a reasonably low dispersity (2.87 ± 0.48 nm). Scale bar in (a) is 10 nm. The IR spectrum (c) shows the symmetric and asymmetric methylene and methyl stretches associated with the capping ligand, consistent with literature analogues. The UV-vis spectrum (d) indicates no presence of a SPR absorbance in the visible region, but a steady increase in absorbance towards higher energy associated with interband transitions. The wide scan X-ray photoelectron spectrum (e) indicates the presence of elemental Cu, C, S and O, whilst the high resolution scan shows Cu $2p^{3/2}$ and $2p^{1/2}$ peaks at 932.43 and 952.23 eV respectively, indicating that the copper is likely to be in the +1 oxidation state as Cu_2O (Cu $2p^{3/2}$ = 932.67 eV, Cu_2O $2p^{3/2}$ = 932.4 eV).

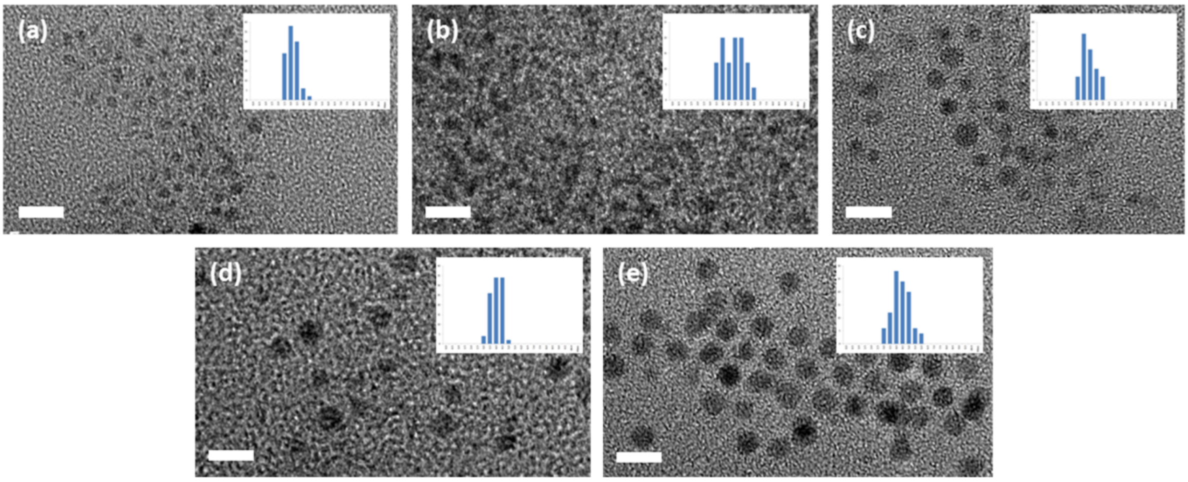

Figure S2. Transmission electron microscopic analysis of the copper, silver and copper-silver alloy nanoparticles: (a) CuNP, (b) CuAgNP (75:25), (c) CuAgNP (50:50), (d) CuAgNP (25:75) and (e) AgNP. The nanoparticles are largely spherical and have a moderately low dispersity. Inset are histograms displaying the corresponding nanoparticle size distribution. Scale bars are 10 nm.

Table S1. Characterisation of the copper, silver and copper-silver alloy nanoparticles: $(d_{NP})_{TEM}$ is the mean diameter of the nanoparticles determined using TEM analyses; $(\lambda_{SPR})_{UVS}$ is the position of the surface plasmon resonance absorbance recorded using UV-vis spectroscopy; $(\nu_{CH})_{IRS}$ are the C-H stretching vibrations recorded using IR spectroscopy; $(\%_{Cu})_{XPS}$ is the atomic percentage of Cu relative to Ag according to XPS.

Catalyst	**$(d_{NP})_{TEM}$ / nm**	**$(\lambda_{SPR})_{UVS}$ / nm [a]**	**$(\nu_{CH})_{IRS}$ / cm^{-1} [b]**	**$(\%_{Cu})_{XPS}$ / % [c]**
CuNP	2.87 ± 0.48	-	2954, 2917, 2872, 2848	100.0
CuAgNP (75:25)	4.58 ± 0.88	463.8	2955, 2920, 2872, 2850	61.3
CuAgNP (50:50)	3.69 ± 0.61	453.3	2953, 2918, 2872, 2849	29.5
CuAgNP (25:75)	3.78 ± 0.40	445.4	2952, 2914, 2872, 2846	16.9
AgNP	4.15 ± 0.69	436.3	2952, 2914, 2872, 2846	-

[a] The characteristic SPR absorbance associated with nanoscale silver is seen to shift to longer wavelength with increasing copper content, consistent with documented experimental and theoretical precedents; [b] All nanoparticle samples exhibit the four characteristic C-H stretching vibrations in the region 2960-2840 cm^{-1} (symmetric and asymmetric methyl and methylene stretches), however no trend in the relative position or intensity of these signatures was observed across samples ; [c] The relative ratio of Cu:Ag recorded using XPS did not exactly match that anticipated from the known stoichiometry of metals in the reaction feedstock, however the trend of increasing %Cu in the product with increasing %Cu in the synthesis mixture was observed.

S3. Synthesis and characterisation of nanoparticle-graphitised nanofibre composites

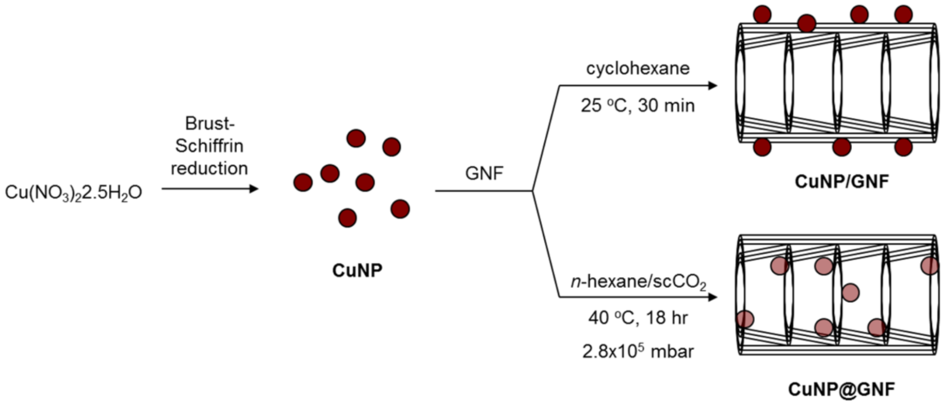

Scheme S1. Strategy for the preparation of the supported copper nanoparticle and nanoreactor catalysts. The use of supercritical carbon dioxide ($scCO_2$) is essential for selective encapsulation of nanoparticles inside nanofibers, as $scCO_2$ possesses properties intermediate of gases and liquids, such as low viscosity, high diffusivity and zero surface tension, and is therefore ideally suited to facilitate the continual and uninhibited movement of adsorbed nanoparticles along the atomically smooth exterior surface of nanofibres and subsequent transport into the interior of GNF. As nanoparticles diffuse to the step-edge, they become spontaneously immobilised due to the maximised van der Waals interactions between the metallic core of the nanoparticle and the underlying graphitic structure of the nanofibre step-edge. Conversely, in the absence of $scCO_2$, nanoparticles adsorb on the exterior surface of nanofibres from organic solution and while diffusion barriers are sufficiently low to allow for surface diffusion, nanoparticles do not become encapsulated and remain on the outer surface.

Adsorption of copper nanoparticles on graphitised nanofibres (CuNP/GNF)

To a solution of copper nanoparticles (0.6 mg) in cyclohexane (10 mL) was added graphitised carbon nanofibres (10 mg, PR-24 GNF, as-received) and the combined mixture was bath sonicated for 30 min at room temperature. The obtained black solid was collected by vacuum filtration (0.2 µm PTFE), washed with cyclohexane (25 mL), chloroform (25 mL) and acetone (25 mL) and sucked dry under vacuum (10.5 mg).

Encapsulation of copper nanoparticles on graphitised nanofibres (CuNP@GNF)

To a solution of copper nanoparticles (0.3 mg) in *n*-hexane (5 mL) was added graphitised carbon nanofibres (5 mg, PR-24 GNF, annealed for 1 hr at 450 ^{o}C in air) and the combined mixture was bath sonicated for 15 min at room temperature. The obtained suspension was transferred to a steel autoclave (10 mL volume) equipped with a magnetic stirrer bar and mixed with carbon dioxide (40 ^{o}C, 4000 psi) for 18 hr. During the course of the experiment, the carbon dioxide pressure was cycled between 1000 and 4000 psi a total of three times. The resulting solid was extracted with ethanol (10 x 5 mL), filtered through a membrane filter (0.2 µm, PTFE), washed with acetone (20 mL), chloroform (20 mL), *n*-hexane (20 mL) and acetone (20 mL) and sucked dry under vacuum. The experiment was duplicated and the black solids combined (9.1 mg).

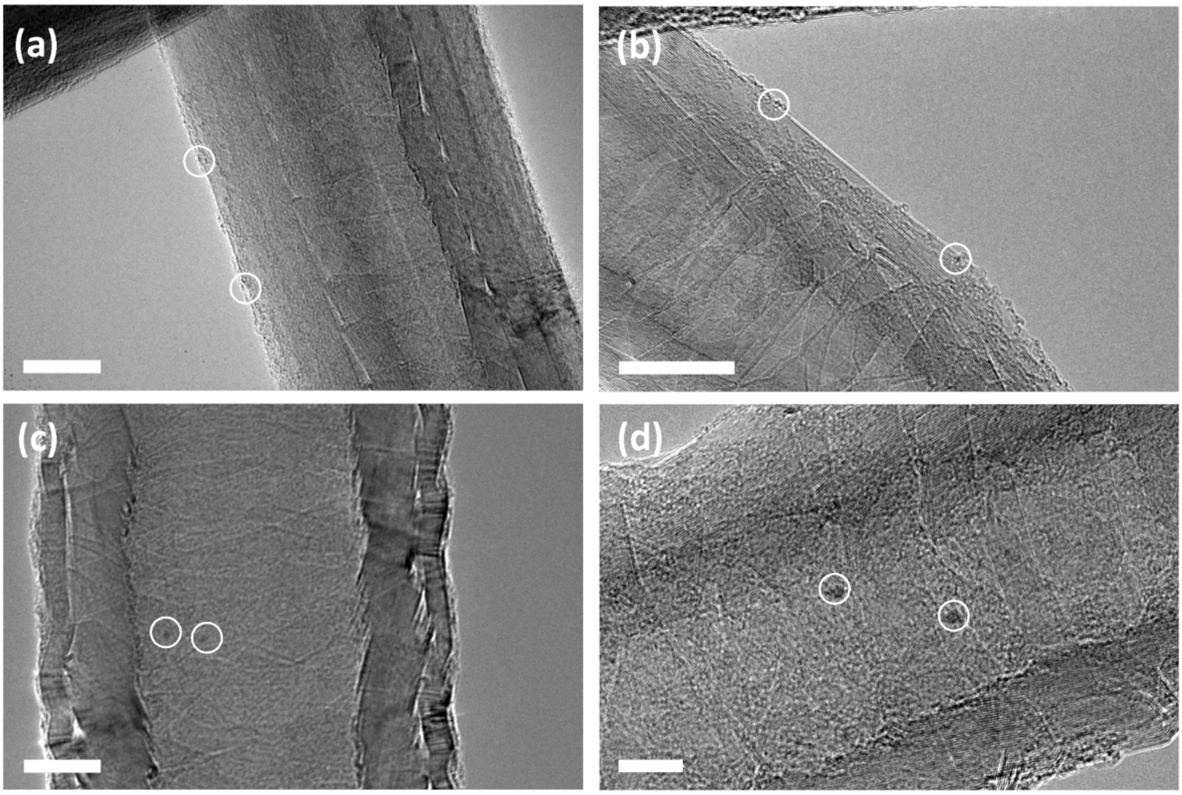

Figure S3. Transmission electron micrographs of the (a-b) supported (CuNP/GNF) and (c-d) nanoreactor (CuNP@GNF) catalysts. The location of surface adsorbed nanoparticles in the CuNP/GNF catalyst is difficult to discern due to the high mobility of nanoparticles on the atomically smooth nanofibre exterior surface, however a loading of 3.8 % was determined by thermogravimetric analysis. A comparable loading of 3.7 % was observed for CuNP@GNF. Scale bars are 20 (a-c) and 10 nm (d).

S4. Synthesis and characterisation of 1,2,3-triazoles

General procedure for 1,3-dipolar cycloaddition of azides to alkynes

To the catalyst (2.5 mol %) was added the alkyne (0.1 mmol), azide (0.1 mmol), triethylamine (0.15 mmol) and a degassed solution of deuterated benzene (1.4 mL) and the combined suspension heated at 40 °C under an inert atmosphere of argon. The catalyst was recovered by vacuum filtration (0.45 µm PTFE), washed with deuterated benzene (5 mL), sucked dry and finally dried over phosphorus pentoxide. The filtrate was concentrated under vacuum and either characterised immediately by ^{1}H NMR spectroscopy or purified by flash chromatography.

Characterisation of [1,2,3]-triazoles

(3a) 1-benzyl-4-(4-nitrophenyl)-1H-[1,2,3]-triazole

White solid; R_f 0.21 (dichloromethane); ^{1}H NMR (C_6D_6) δ_H/ppm 7.89 (d, 2H, J = 8.9 Hz), 7.46 (d, 2H, J = 8.9 Hz), 7.00 (m, 3H), 6.81 (m, 3H), 6.70 (s, 1H), 4.79 (s, 2H); ^{1}H NMR (CD_3OD) δ_H/ppm 8.15 (d, 2H, J = 8.7 Hz), 7.49 (d, 2H, J = 8.7 Hz), 7.35 (m, 6H), 5.66 (s, 2H); ^{1}H NMR ($CDCl_3$) δ_H/ppm 8.26 (d, 2H, J = 8.2 Hz), 7.97 (d, 2H, J = 8.2 Hz), 7.82 (s, 1H), 7.42 (m, 3H), 7.35 (m, 2H), 5.61 (s, 2H); ^{13}C NMR ($CDCl_3$) δ_C/ppm 147.27, 145.98, 136.76, 134.13, 129.27, 129.04, 128.16, 126.09, 124.23, 120.94, 54.44; HRMS *m/z* calculated for $C_{15}H_{13}N_4O_2$ 281.1039, found 281.1027 $[M+H]^+$.

(3b) 1-benzyl-4-(4-bromophenyl)-1H-[1,2,3]-triazole

White solid; R_f 0.47 (dichloromethane); ^{1}H NMR (C_6D_6) δ_H/ppm 7.47 (d, 2H, J = 8.7 Hz), 7.29 (d, 2H, J = 8.7 Hz), 6.99 (m, 3H), 6.81 (m, 2H), 6.73 (s, 1H), 4.81 (s, 2H); ^{1}H NMR ($CDCl_3$) δ_H/ppm 7.66 (d, 2H, J = 8.7 Hz), 7.66 (s, 1H), 7.51 (d, 2H, J = 8.7 Hz), 7.39 (m, 3H), 7.31 (m, 2H), 5.57 (s, 2H); ^{13}C NMR ($CDCl_3$) δ_C/ppm 147.14, 134.44, 131.90, 129.46, 129.17, 128.84, 128.07, 127.17, 121.99, 119.53, 54.26; HRMS *m/z* calculated for $C_{15}H_{13}N_3Br$ 314.0287, found 314.0277 $[M+H]^+$.

(3c) 1-benzyl-4-phenyl-1H-[1,2,3]-triazole

White solid; R_f 0.29 (dichloromethane); ^{1}H NMR (C_6D_6) δ_H/ppm 7.86 (m, 2H), 7.19 (m, 3H), 6.98 (m, 3H), 6.87 (s, 1H), 6.83 (m, 2H), 4.83 (s, 2H); ^{1}H NMR ($CDCl_3$) δ_H/ppm 7.81 (m, 2H), 7.67 (s, 1H), 7.41 (m, 5H), 7.32 (m, 3H), 5.59 (s, 2H); ^{13}C NMR ($CDCl_3$) δ_C/ppm 148.23, 134.67, 130.52, 129.15, 128.79, 128.16, 128.05, 125.69, 119.45, 54.23; HRMS *m/z* calculated for $C_{15}H_{14}N_3$ 236.1182, found 236.1187 $[M+H]^+$.

(3d) 1-benzyl-4-(4-methoxyphenyl)-1H-[1,2,3]-triazole

White solid; R_f 0.21 (dichloromethane); ^{1}H NMR (C_6D_6) δ_H/ppm 7.82 (d, 2H, J = 8.9 Hz), 6.99 (m, 3H), 6.84 (m, 5H), 4.86 (s, 2H), 3.29 (s, 3H); ^{1}H NMR ($CDCl_3$) δ_H/ppm 7.63 (d, 2H, J = 8.1 Hz), 7.49 (s, 1H), 7.21 (m, 5H), 6.83 (d, 2H, J = 8.1 Hz), 5.46 (s, 2H), 3.73 (s, 3H); ^{13}C NMR ($CDCl_3$) δ_C/ppm 159.55, 148.38, 134.74, 129.09, 128.70, 128.04, 126.95, 123.26, 118.80, 114.16, 55.26, 54.15; HRMS *m/z* calculated for $C_{16}H_{16}N_3O$ 266.1293, found 266.1282 $[M+H]^+$.

(3e) 1-benzyl-4-(4-aminophenyl)-1H-[1,2,3]-triazole

White solid; R_f 0.38 (dichloromethane / ethyl acetate, 3 / 1); ^{1}H NMR (C_6D_6) δ_H/ppm 7.75 (d, 2H, *J* = 8.6 Hz), 6.98 (m, 3H), 6.85 (s, 1H), 6.83 (m, 2H), 6.33 (d, 2H, *J* = 8.6 Hz), 4.83 (s, 2H); ^{1}H NMR ($CDCl_3$) δ_H/ppm 7.60 (d, 2H, *J* = 8.7 Hz), 7.53 (s, 1H), 7.38 (m, 3H), 7.31 (m, 2H), 6.71 (d, 2H, *J* = 8.7 Hz), 5.55 (s, 2H); ^{13}C NMR ($CDCl_3$) δ_C/ppm 148.54, 146.45, 134.84, 129.08, 128.66, 128.00, 126.90, 121.05, 118.18, 115.19, 54.12; HRMS *m/z* calculated for $C_{15}H_{15}N_4$ 251.1297, found 251.1294 $[M+H]^+$.

(3f) 1-benzyl-4-(4-cyclohexyl)-1H-[1,2,3]-triazole

White solid; R_f 0.24 (dichloromethane); ^{1}H NMR (C_6D_6) δ_H/ppm 6.97 (m, 3H), 6.85 (m, 2H), 6.54 (s, 1H), 4.86 (s, 2H), 2.73 (m, 1H), 2.05 (m, 2H), 1.62 (m, 4H), 1.37 (m, 4H); ^{1}H NMR ($CDCl_3$) δ_H/ppm 7.39 (m, 3H), 7.28 (m, 2H), 7.17 (s, 1H), 5.51 (s, 2H), 2.76 (m, 1H), 2.05 (m, 2H), 1.78 (m, 4H), 1.39 (m, 4H); ^{13}C NMR ($CDCl_3$) δ_C/ppm 154.18, 134.96, 129.03, 128.57, 128.00, 119.17, 54.00, 35.30, 32.97, 26.10, 26.00; HRMS *m/z* calculated for $C_{15}H_{20}N_3$ 242.1652, found 242.1653 $[M+H]^+$.

(3g) 1-benzyl-4-(*n*-octyl)-1H-[1,2,3]-triazole

White solid; R_f 0.40 (dichloromethane); ^{1}H NMR (C_6D_6) δ_H/ppm 7.09 (m, 3H), 6.96 (m, 2H), 6.60 (s, 1H), 4.97 (s, 2H), 2.78 (t, 2H, *J* = 7.6 Hz), 1.75 (qn, 2H, *J* = 7.6 Hz), 1.34 (m, 10H), 1.00 (t, 3H, *J* = 6.6 Hz); ^{1}H NMR ($CDCl_3$) δ_H/ppm 7.39 (m, 3H), 7.27 (m, 2H), 7.20 (s, 1H), 5.51 (s, 2H), 2.70 (t, 2H, *J* = 7.6 Hz), 1.66 (qn, 2H, *J* = 7.6 Hz), 1.33 (m, 10H), 0.89 (t, 3H, *J* = 6.7 Hz); ^{13}C NMR ($CDCl_3$) δ_C/ppm 148.96, 134.98, 129.02, 128.56, 127.92, 120.45, 53.96, 31.83, 29.38, 29.28, 29.23, 29.16, 25.70, 22.62, 14.07; HRMS *m/z* calculated for $C_{17}H_{26}N_3$ 272.2121, found 272.2118 $[M+H]^+$.

(3h) 1-(1-benzyl-1H-[1,2,3]-triazol-4-yl)methanol

White solid; R_f 0.46 (ethyl acetate); ^{1}H NMR (C_6D_6) δ_H/ppm 6.97 (m, 3H), 6.80 (m, 2H), 6.62 (s, 1H), 4.77 (s, 2H), 4.56 (s, 2H); ^{1}H NMR ($CDCl_3$) δ_H/ppm 7.46 (s, 1H), 7.38 (m, 3H), 7.29 (m, 2H), 5.53 (s, 2H), 4.78 (s, 2H); ^{13}C NMR ($CDCl_3$) δ_C/ppm 148.02, 134.43, 129.13, 128.80, 128.11, 121.57, 56.50, 54.20; HRMS *m/z* calculated for $C_{10}H_{12}N_3O$ 190.0975, found 190.0990 $[M+H]^+$.

(3i) 1-hexyl-4-(4-nitrophenyl)-1H-[1,2,3]-triazole

White solid; R_f 0.47 (dichloromethane); ^{1}H NMR (C_6D_6) δ_H/ppm 7.94 (d, 2H, *J* = 8.9 Hz), 7,61 (d, 2H, J = 8.9 Hz), 6.68 (s, 1H), 3.64 (t, 2H, *J* = 7.3 Hz), 1.37 (qn, 2H, *J* = 7.3 Hz), 1.12 (qn, 2H, *J* = 7.3 Hz), 1.08 (m, 4H), 0.82 (t, 3H, *J* = 5.3 Hz); ^{1}H NMR (C_6D_6) δ_H/ppm 8.29 (d, 2H, *J* = 9.0 Hz), 8.01 (d, 2H, *J* = 9.0 Hz), 7.91 (s, 1H), 4.44 (t, 2H, *J* = 7.2 Hz), 1.98 (qn, 2H, *J* = 7.2 Hz), 1.35 (m, 6H), 0.89 (t, 3H, *J* = 5.4 Hz); ^{13}C NMR δ_C/ppm 147.25, 145.53, 136.98, 126.07, 124.29, 120.87, 50.67, 31.10, 30.25, 26.12, 22.38, 13.90; HRMS *m/z* calculated for $C_{14}H_{19}N_4O_2$ 275.1503, found 275.1497 $[M+H]^+$.

S5. Observation of the Hammett relationship

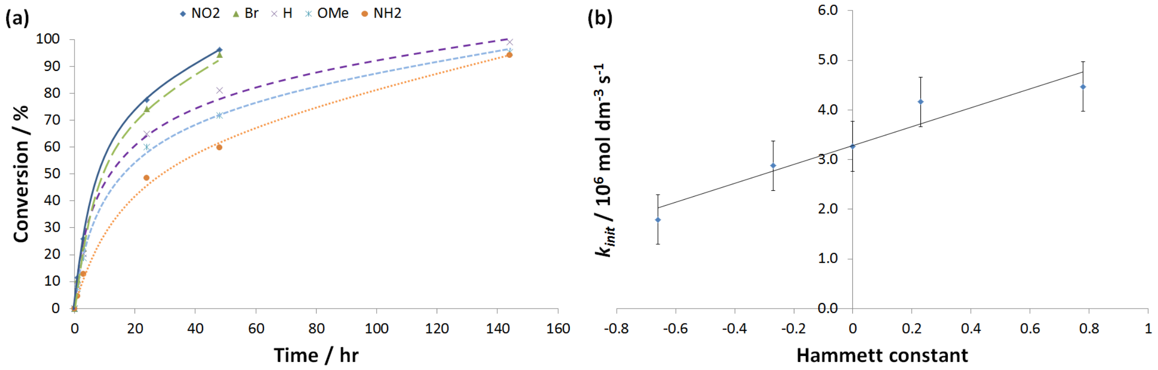

Figure S4. (a) Reaction kinetics and (b) the linear relationship between the initial reaction rate (k_{init}) and the Hammett constant for the series of *para*-substituted phenylacetylenes investigated in this study. The initial reaction rate is an approximate based on the formation of 1,2,3-triazole product at t = 1 hr as determined by ^{1}H NMR spectroscopy.

S6. The effect of recycling on the morphology of the catalyst

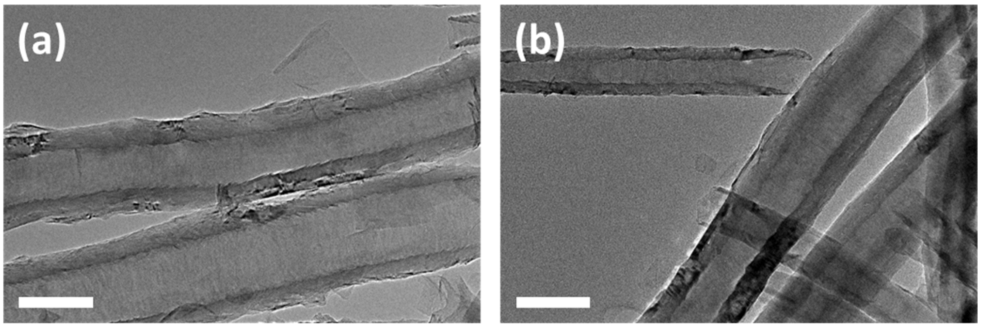

Figure S5. TEM of the supported CuNP/GNF catalyst after five cycles, indicating almost total loss of metallic copper, confirmed by a significant reduction in the copper loading (0.4 % by TGA). Scale bars are 100 nm.

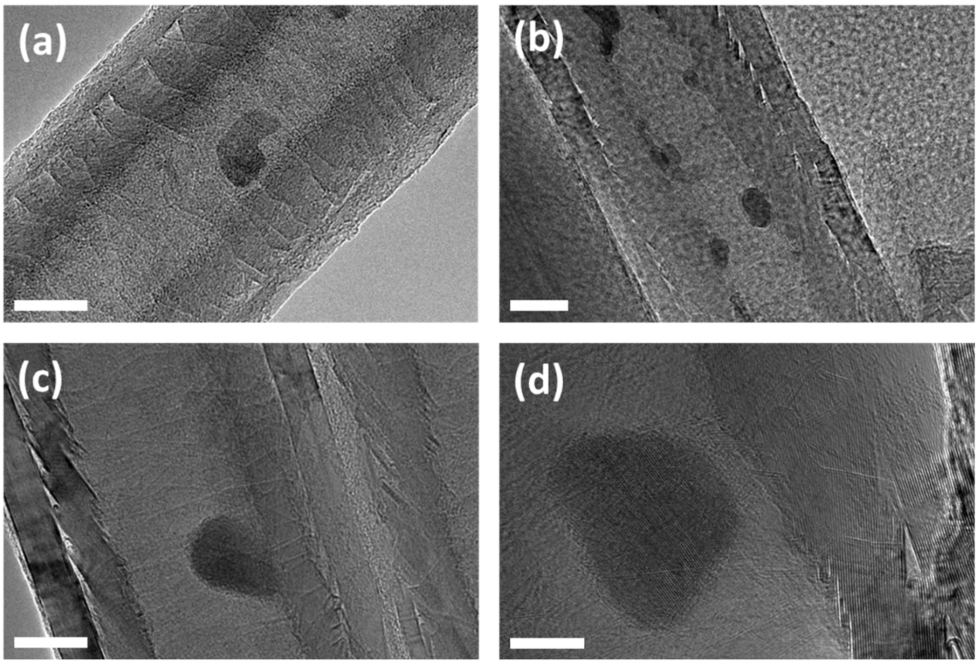

Figure S6. CuNP@GNF after 5 catalytic cycles showing the *in situ* ripening of the copper nanoparticle catalysts. Scale bars are 20 (a-c) and 10 nm (d). Only a minimal loading loss was observed from TGA (2.8 %).

S7. Effect of nanoparticle ripening on catalytic recycling

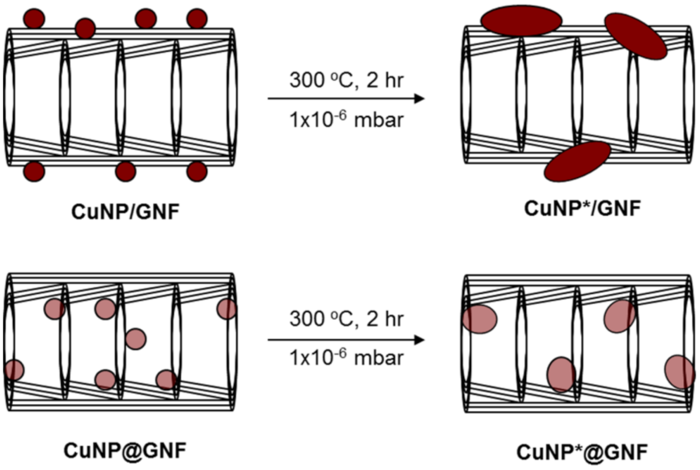

Scheme S2. Strategy for the preparation of the ripened nanoreactor catalysts.

Ripening of nanoparticle-nanofibre composites

The composite was sealed in a Pyrex tube at 5×10^{-6} mbar and heated for 2 hr at 300 °C.

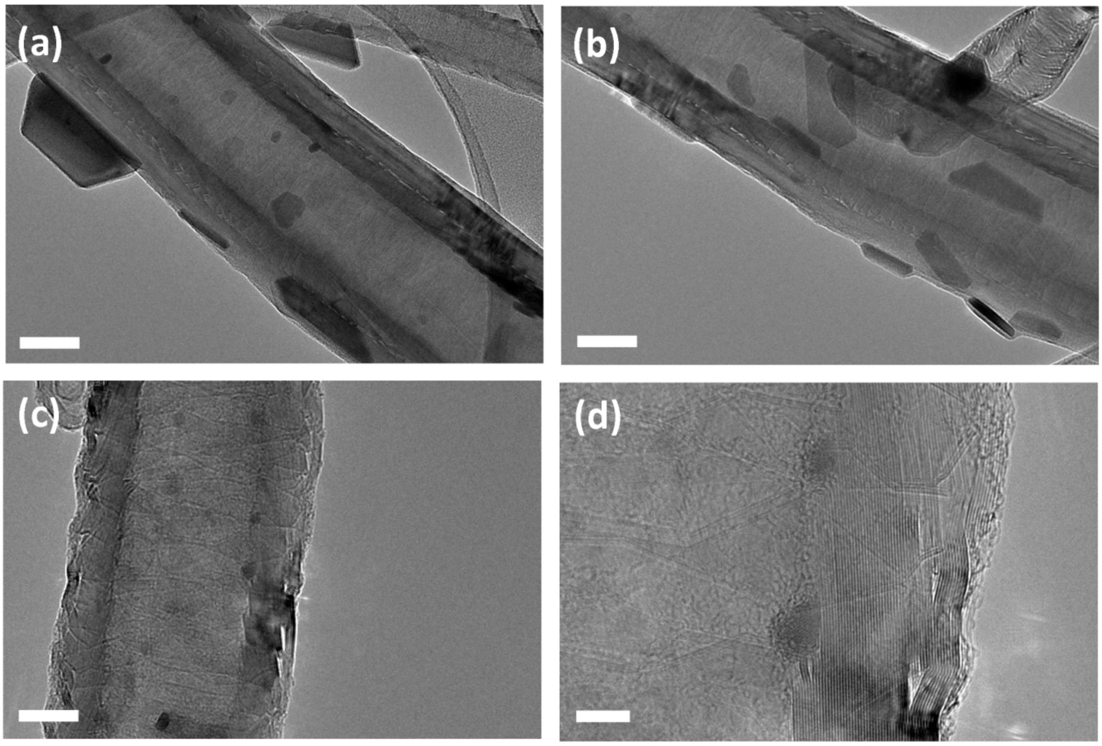

Figure S7. TEM analysis of the (a-b) ripened supported (CuNP*/GNF) and (c-d) nanoreactor (CuNP*@GNF) catalysts. The small spherical as-prepared nanoparticles were transformed into trapezoidal and rod-like nanoparticles (*ca.* 70x30x15 nm) on the exterior surface and pseudo-spherical particulates (*ca.* 8.5 nm in diameter) in the inner cavity. Due to the unambiguous nature of the location of the ripened nanoparticles, these samples also aided our attempts to quantify the ratio of externally/internally adsorbed nanoparticles. From statistical analysis of multiple micrographs, we observed that in excess of 80% of nanoparticles are on the outer surface for the supported catalysts and more than 90% are confined within the internal channel for the nanoreactor systems. Critically the ripened nanoparticles remain confined at the internal step-edges as seen in (d).

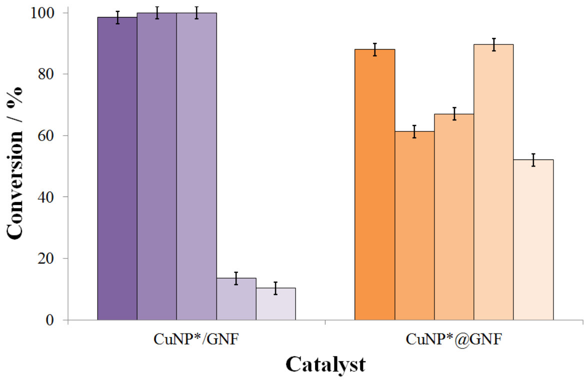

Figure S8. The recyclability of the ripened supported (CuNP*/GNF) and nanoreactor (CuNP*@GNF) catalysts, showing the near total loss of catalytic activity of the supported catalyst after three cycles and high, stable activity and recyclability over five cycles for the nanoreactor catalyst, highlighting the importance of nanoparticle encapsulation in graphitised nanofibres for effective catalyst recycling.

S8. References

[S1] D.V. Kosynkin, J.M. Tour, *Org. Lett.* **2001**, *3*, 993-996.

[S2] D.L. Pearson, J.M. Tour, *J. Org. Chem.* **1997**, *62*, 1376-1387.

[S3] D.-R. Hou, T.-C. Kuan, Y.-K. Li, L. Richmond, K.-W. Huang, *Tetrahedron* **2010**, *66*, 9415-9420.

[S4] J.S. Garitaonandia, M. Insausti, E. Goikolea, M. Suzuki, J.D. Cashion, N. Kawamura, H. Ohsawa, I. Gil de Muro, K. Suzuki, F. Plazaola, T. Rojo, *Nano Lett.* **2008**, *8*, 661-667.

[S5] M. Brust, M. Walker, D. Bethell, D.J. Schiffrin, R. Whyman, *J. Chem. Soc. Chem. Comm.* **1994**, 801-802.

[S6] T.P. Ang, W.S. Chin, *J. Phys. Chem. C* **2005**, *109*, 22228-22236.